**University of Wisconsin - Madison**

**MADPH-00-1208**
**FERMILAB-Pub-00/332-T**
hep-ph/0012351
December 2000

# $H \to WW$ as the discovery mode for a light Higgs boson

N. Kauer[1], T. Plehn[1], D. Rainwater[2] and D. Zeppenfeld[1]

[1] *Department of Physics, University of Wisconsin, Madison, WI 53706*
[2] *Fermi National Accelerator Laboratory, Batavia, IL 60510*



## Abstract

The production cross section for a $m_H \approx 115$ GeV, SM Higgs boson in weak boson fusion at the LHC is sizable. However, the branching fraction for $H \to W^+W^-$ is expected to be relatively small. The signal, with its two forward jets, is sufficiently different from the main backgrounds that a signal to background ratio of better than 1:1 can nevertheless be obtained, with large enough rate to allow for a $5\sigma$ signal with 35 fb$^{-1}$ of data. The $H \to WW$ signal in weak boson fusion may thus prove to be the discovery mode for the Higgs boson at the LHC.

After the end of LEP II running, the search for the Higgs boson and, hence, for the origin of electroweak symmetry breaking and fermion mass generation, remains one of the premier tasks of present and future high energy physics experiments. With the exclusion of a SM Higgs boson of mass $m_H < 113.5$ GeV and some evidence for $m_H \approx 115$ GeV [1], the mass range now preferred by supersymmetry [2,3], 113 GeV$\lesssim m_h \lesssim 130$ GeV, will likely remain the focus of investigations until the beginning of data taking at the CERN LHC.

Previously we have shown that a somewhat heavier Higgs boson, in the range 130 GeV$\lesssim m_H \lesssim$ 190 GeV, will give a highly significant $H \to W^+W^- \to e^\pm\mu^\mp \not{p}_T$ signal in weak boson fusion (WBF) at the LHC [4,5]. For a smaller Higgs boson mass, the branching ratio of the $H \to W^+W^-$ mode quickly decreases, making the observation of this mode more difficult. Only a marginal signal was expected for $m_H \approx 115$ GeV. However, this earlier analysis was optimized for a Higgs boson mass near $W$-pair threshold and can clearly be improved for the significantly smaller masses favored at the end of LEP II running. This situation motivates a complete reanalysis of possible $H \to W^+W^-$ signals in WBF at the LHC, and of possible backgrounds, with the goal of optimizing the significance of a signal for $m_H \approx 115$ GeV. At the same time a better signal to background ($S/B$) ratio, higher signal acceptance and higher accuracy in the determination of $B\sigma(qq \to qqH,\ H \to WW)$ would significantly improve the extraction of Higgs boson properties such as its total width or the $HWW$ coupling constant [6].

In this letter we summarize the results of this reanalysis, and show that even for a SM Higgs of

$m_H = 115$ GeV the $H \to WW$ decay mode can be observed in WBF, with better than $5\sigma$ significance, with about 35 fb$^{-1}$ of LHC data. This result of our parton level analysis, if confirmed by a more complete simulation of hadronization and detector effects, would render this WBF mode the most promising single search channel at the LHC, superior even to the classic inclusive search for a $H \to \gamma\gamma$ resonance peak [7,8].

Our results are based on parton level simulations of the signal and the various backgrounds, with full tree level matrix elements of all contributing subprocesses. Thus, final state partons are identified with observable jets. The signal can be described as the scattering of quarks and/or anti-quarks via $t$-channel $W$ and $Z$-exchange, with the Higgs boson radiated off this weak boson. The signal contains two (forward) quark-jets, called tagging jets, in addition to the $H \to W^+W^- \to ll'\nu\bar{\nu}$ decay products. Here, one or both $W$ bosons may be virtual. We consider $ll' = e^\pm\mu^\mp$ and also $ll' = e^+e^-,\ \mu^+\mu^-$ final states. The latter, dubbed 'same flavor' or $ll$ sample, were not considered in Refs. [4,5].

Any processes resulting in two jets, two (oppositely) charged leptons and missing transverse momentum constitute potential backgrounds. The dominant background turns out to be top-quark pair production in association with up to two additional light-quark or gluon jets. For the $t\bar{t}$ and $t\bar{t}j$ simulation we use the results of Ref. [9] which include off-shell top and $W$ effects and take into account the single-resonant and non-resonant contributions. This inclusion is potentially important since, for the Higgs masses considered here, the $ll'\nu\bar{\nu}$ final state is produced well below threshold for $t\bar{t}$ decays. The top-quark backgrounds are separated into three categories, depending on whether two, one or zero $b$ (or $\bar{b}$) quarks are identified as one of the two forward tagging jets, and are called $tt$, $ttj$ and $ttjj$ backgrounds, respectively.

$W$-pair production in association with two light partons constitutes the next major background. The 'QCD $WWjj$' background is calculated at order $\mathcal{O}(\alpha^2\alpha_s^2)$ and contains the real emission corrections to $q\bar{q} \to W^+W^-$ (and crossing related processes). The 'EW $WWjj$' background consists of all $q_1q_2 \to q_3q_4W^+W^-$ processes at order $\mathcal{O}(\alpha^4)$. Similarly, the 'QCD $\tau\tau jj$' and 'EW $\tau\tau jj$' backgrounds capture $\tau$-pair production in association with two jets at $\mathcal{O}(\alpha_s^2\alpha^2)$ and $\mathcal{O}(\alpha^4)$, respectively, with subsequent leptonic $\tau$-decay. They include full $Z, \gamma$ interference effects. Finally, the '$bbjj$' background arises from $b\bar{b}jj$ production (simulated at $\mathcal{O}(\alpha_s^4)$), with semi-leptonic decays of both bottom quarks. The simulation of these backgrounds is performed as in Refs. [4,10]. For the same flavor sample we also consider QCD $ZZjj$ final states with $ZZ \to l^+l^-\nu\bar{\nu}$ (generated like the QCD $WWjj$ background and including $\gamma^* \to l^+l^-$ contributions); and QCD and EW $lljj$ final states, which are calculated like the $\tau\tau jj$ backgrounds, except that the missing transverse momentum is now entirely due to detector effects, which are simulated as in Ref. [4].

The basic event selection which we propose is similar to the one suggested previously [4]. One looks for events with at least two jets (tagging jets) and two charged leptons in the phase space region

$$\begin{aligned} p_{Tj} \geq 20 \text{ GeV}\,, \quad |\eta_j| \leq 4.5\,, \quad \triangle R_{jj} \geq 0.6\,, \\ p_{T\ell_1} \geq 20 \text{ GeV}\,,\ p_{T\ell_2} \geq 10 \text{ GeV}\,, \quad |\eta_\ell| \leq 2.5\,, \quad \triangle R_{j\ell} \geq 1.7\,. \end{aligned} \tag{1}$$

The staggered lepton $p_T$ cut accommodates the softer lepton from the decay of a virtual $W$. Both charged leptons must lie between the tagging jets with a separation in pseudorapidity $\triangle\eta_{j,\ell} > 0.6$, and the jets must occupy opposite hemispheres:

$$\begin{aligned} \eta_{j,min} + 0.6 < \eta_{\ell_{1,2}} < \eta_{j,max} - 0.6\,, \\ \eta_{j_1} \cdot \eta_{j_2} < 0\,. \end{aligned} \tag{2}$$

A large dijet invariant mass and a wide separation in pseudorapidity is required for the two forward tagging jets,

$$m_{jj} > 600 \text{ GeV}\,, \qquad \triangle\eta_{tags} = |\eta_{j_1} - \eta_{j_2}| \geq 4.2\,, \tag{3}$$

leaving a gap of at least 3 units of pseudorapidity in which the charged leptons can be observed.

Forward jet tagging has been discussed as an effective technique to separate weak boson scattering from various backgrounds in the past [11–15,4,5], in particular for heavy Higgs boson searches. A second technique for suppression of QCD backgrounds to WBF is the veto of any additional identifiable jet activity in the central region [14,15]. We discard all events where an additional veto jet of $p_{Tv} > 20$ GeV is located in the gap region between the two tagging jets,

$$p_{Tv} > 20 \text{ GeV}\,, \quad \eta_{j,min} < \eta_v < \eta_{j,max}\,. \tag{4}$$

First of all the jet veto is very effective against the $t\bar{t}$ backgrounds, by vetoing most of the relatively hard $b$ and $\bar{b}$ arising from top-quark decay [7,8]. In addition, the central jet veto exploits the different gluon radiation patterns of WBF, where most additional partons will be emitted in the far forward and far backward directions, and of $t$-channel gluon exchange processes, which prefer additional parton emission in the central region. We do not explicitly generate these additional soft jets in our parton level Monte Carlo programs. Their effect has been estimated in Refs. [4,5,15] and can be included as overall veto survival probabilities of $P_{surv} = 0.89$ for the Higgs signal, 0.29 for the QCD backgrounds (including $t\bar{t}$ production) and 0.75 for the EW backgrounds. There is some uncertainty in these estimates and they will eventually have to be determined experimentally, from LHC data on $Wjj$ and $Zjj$ production [15]. We therefore include these survival probabilities only at the final stage of the analysis.

The two (virtual) $W$s of the Higgs boson signal are produced close to threshold and are almost at rest in the Higgs frame. As a result, the charged lepton and the neutrino arising from a single $W$ are almost back-to-back in this frame, and they have equal energies. This implies that the invariant masses of the two charged leptons and of the two neutrinos are approximately equal, $m_{ll} \approx m_{\nu\bar{\nu}}$, and neither can exceed half the Higgs boson mass. In the lab frame the relatively small dilepton invariant mass favors a small angle between the two charged leptons. Since we are interested in Higgs boson masses $m_H \lesssim 130$ GeV, we require

$$m_{ll} < 60 \text{ GeV}\,, \quad \phi_{ll} < 140^o\,, \tag{5}$$

where $\phi_{ll}$ is the azimuthal angle between the charged leptons. Small angular separations of the leptons are further favored by the tensor structure of the SM $HWW$ coupling [16,4]. These cuts still leave a large background from $\tau$-pairs. For $\tau^+\tau^-$ events the energy fractions $x_{\tau_1}$, $x_{\tau_2}$ carried by the observed $\tau$-decay leptons can be determined from transverse momentum balance, $\mathbf{p}_{T\tau_1} + \mathbf{p}_{T\tau_2} = \mathbf{p}_{Tl_1} + \mathbf{p}_{Tl_2} + \not{\mathbf{p}}_T$, and thus the $\tau$-pair invariant mass, $m_{\tau\tau} = m_{ll}/\sqrt{x_{\tau_1} x_{\tau_2}}$ can be reconstructed [17]. We veto any events consistent with $Z \to \tau\tau$, i.e. events which satisfy the three conditions

$$x_{\tau_1} > 0\,, \qquad x_{\tau_2} > 0\,, \qquad m_{\tau\tau} > m_Z - 25 \text{ GeV}\,. \tag{6}$$

Positive identification of the Higgs boson is greatly aided by the reconstruction of a Higgs mass peak. Because of the two missing neutrinos in the decay of the two $W$s the invariant mass of the Higgs decay products cannot be reconstructed.[1] However, it is possible to reconstruct the transverse mass of the

[1] In the threshold approximation, i.e. neglecting the $W^\pm$ momenta in the Higgs rest frame, and assuming one $W$ to be on-shell, the Higgs mass can be reconstructed, with, typically, a two-fold ambiguity. We find that this reconstruction is less efficient for rejecting backgrounds than the $WW$ transverse mass.

TABLE I. Signal and background cross sections (in fb) within the cuts indicated. The first four columns refer to $e\mu\not{p}_T$ final states, while the last column gives results, after all the cuts of Eqs. (1–11), for the $ll = ee,\ \mu\mu$ sample. The survival probabilities for a central jet veto are factored into the cross sections of the last two columns. In the first three columns the central jet veto is only applied to $b$-quark jets from top decay.

| channel | Eqs. (1–8) | + Eq. (9) | + Eq. (10) | $\times P_{surv}$ | same flavor |
|---|---|---|---|---|---|
| $m_H = 115$ GeV | 1.04 | 0.93 | 0.92 | 0.83 | 0.58 |
| $t\bar{t}$ | 0.051 | 0.040 | 0.040 | 0.012 | 0.010 |
| $t\bar{t}j$ | 1.54 | 1.34 | 1.33 | 0.39 | 0.29 |
| $t\bar{t}jj$ | 0.31 | 0.27 | 0.27 | 0.078 | 0.065 |
| $b\bar{b}jj$ | 20.8 | 0.48 | 0.013 | 0.004 | $< 0.001$ |
| QCD $WWjj$ | 0.26 | 0.23 | 0.23 | 0.066 | 0.054 |
| EW $WWjj$ | 0.19 | 0.17 | 0.17 | 0.125 | 0.103 |
| QCD $\tau\tau jj$ | 0.67 | 0.11 | 0.10 | 0.032 | 0.028 |
| EW $\tau\tau jj$ | 0.118 | 0.026 | 0.024 | 0.018 | 0.018 |
| QCD $\ell\ell jj$ | | | | | 0.086 |
| EW $\ell\ell jj$ | | | | | 0.016 |
| $ZZjj$ | | | | | $< 0.001$ |

$ll\not{p}_T$ system by using the threshold relationship $m_{\nu\nu} = m_{ll}$. The transverse mass can then be defined as [4]

$$M_T(WW) = \sqrt{(\not{E}_T + E_{T,ll})^2 - (\mathbf{p}_{T,ll} + \not{\mathbf{p}}_T)^2}\,, \tag{7}$$

with the transverse energies given by $E_{T,ll} = \sqrt{\mathbf{p}_{T,ll}^2 + m_{ll}^2}$ and $\not{E}_T = \sqrt{\not{\mathbf{p}}_T^2 + m_{ll}^2}$. The Higgs signal is largely concentrated in the region

$$50 \text{ GeV} < M_T(WW) < m_H + 20 \text{ GeV}\,. \tag{8}$$

The first column of Table I gives the cross sections for a Higgs signal of mass 115 GeV and the various backgrounds within the cuts of Eqs. (1–8). In addition to a sizable $t\bar{t}$+jets background, the $bbjj$ background sticks out. It arises from semi-leptonic $b \to cl\nu$ decays in which little energy is carried by the charm quark and other hadronization products. There are many ways to reduce this background, e.g. by imposing harder cuts on $\not{p}_T$, or the transverse momenta of the tagging jets or the reconstructed Higgs, by looking for displaced decay vertices, by tightening lepton isolation cuts, etc.

Within our parton level simulation we find that the most efficient way to effectively eliminate the $bbjj$ and also the $\tau\tau jj$ backgrounds is to exploit correlations between lepton azimuthal angles and the transverse momentum of the reconstructed Higgs boson, $p_{TH} = |\mathbf{p}_{Tl_1} + \mathbf{p}_{Tl_2} + \not{\mathbf{p}}_T|$. In $b\bar{b}$ and $\tau^+\tau^-$ decays, missing transverse momentum arises from neutrinos which are emitted parallel to the observed charged leptons. As a result the $\not{\mathbf{p}}_T$-vector lies between the two lepton transverse momentum vectors, and, hence, close to their sum, $\mathbf{p}_{Tll} = \mathbf{p}_{Tl_1} + \mathbf{p}_{Tl_2}$. In the Higgs signal, on the other hand, the two leptons are emitted close to each other in the Higgs rest frame [16] with the neutrinos recoiling against them. These features are captured by the azimuthal angle, $\Delta\phi(ll, \not{p}_T)$, between $\mathbf{p}_{Tll}$ and $\not{\mathbf{p}}_T$. The $bbjj$ and $\tau\tau jj$ backgrounds are concentrated at small values of $\Delta\phi(ll, \not{p}_T)$ while the signal favors large

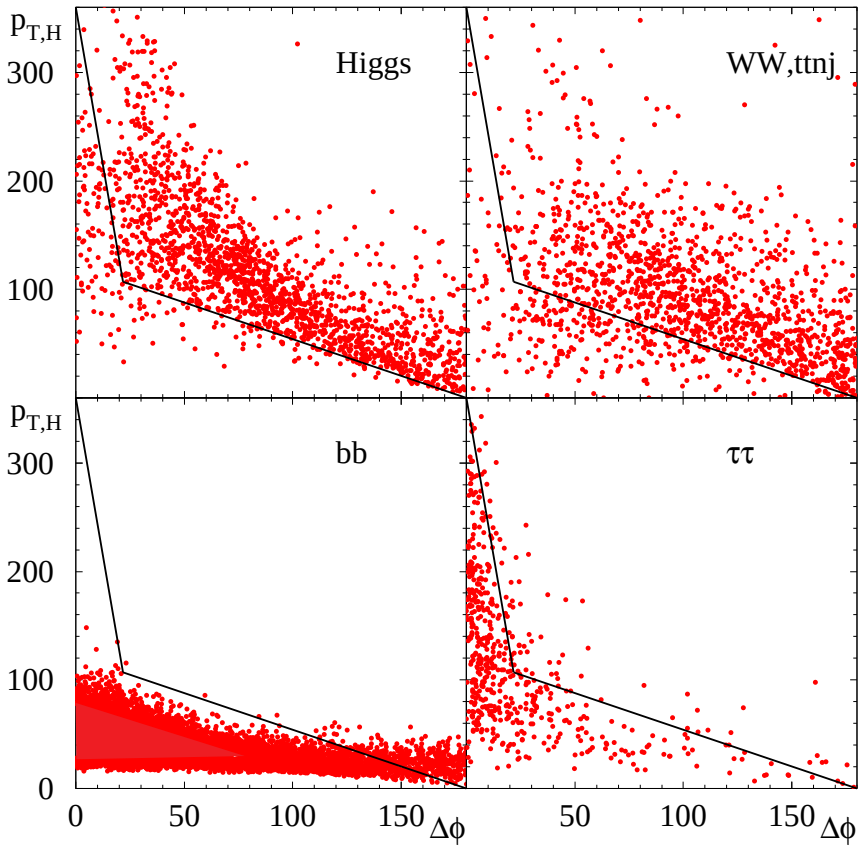


FIG. 1. Distribution of events in the $\Delta\phi(ll, \not{p}_T)$ vs. $p_{TH}$ plane, where $\Delta\phi(ll, \not{p}_T)$ is the azimuthal angle between the dilepton momentum and the missing transverse momentum. Event numbers correspond to 2000 fb$^{-1}$ and the cuts of Eqs. (1–8) and include suppression factors from a central jet veto on extra parton radiation above $p_T = 20$ GeV. The four panels represent a $m_H = 115$ GeV signal, the combined $W^+W^-$ backgrounds from $WWjj$ and $t\bar{t}$+jets sources, the $bbjj$ background and the combined $\tau\tau jj$ backgrounds. Events below and to the left of the straight lines are eliminated by the contour cuts of Eq. (9).

separations, except when a large transverse momentum boost of the Higgs decay products moves them close together.

These correlations are clearly visible in the scatter plots of Fig. 1, which show the expected distribution of events for 2000 fb$^{-1}$ of data in the $\Delta\phi(ll, \not{p}_T)$ vs. $p_{TH}$ plane. While backgrounds arising from $W^+W^-$ decay look very similar to the signal (due to the $m_{ll}$ and $M_T(WW)$ cuts of Eqs. (5,8)) the $bbjj$ and $\tau\tau jj$ backgrounds are concentrated at small $\Delta\phi(ll, \not{p}_T)$ and/or small $p_{TH}$ and are effectively eliminated, with little loss for the signal, by imposing the 'contour cuts'

$$\Delta\phi(ll, \not{p}_T) + 1.5 p_{TH} > 180\ , \qquad 12\Delta\phi(ll, \not{p}_T) + p_{TH} > 360\ , \tag{9}$$

with $\Delta\phi(ll, \not{p}_T)$ measured in degrees and $p_{TH}$ measured in GeV. The resulting cross sections are listed in the second column of Table I.

It is obvious from Fig. 1 that the $bbjj$ background is concentrated at low $p_{TH}$: the charm-quarks from

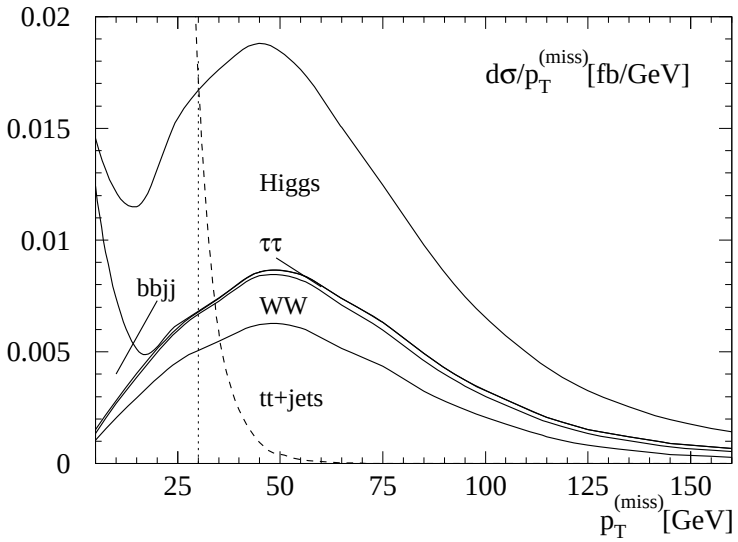


FIG. 2. Missing transverse momentum distribution, $d\sigma/d\not{p}_T$, after the cuts of Eqs. (1–9) for $l^+l^-\not{p}_T$ events. The areas between curves represent the contributions from the various background classes, as indicated, and the signal. QCD and EW backgrounds and the $t\bar{t}$ backgrounds have been combined for clarity. The $l^+l^-jj$ background is indicated by the dashed curve. The vertical line represents the cut of Eq. (11).

$b$-decay will usually not pass the lepton isolation cuts of $E_{Tc} < 5$ GeV [10] unless the parent $b$-quark, and, hence, the decay leptons are soft. This leads to a small charged lepton $p_T$ and, simultaneously, to small $\not{p}_T$ from escaping neutrinos. For large angles $\Delta\phi(ll, \not{p}_T)$, the missing transverse momentum is dominated by mismeasurement in the detector, which is small and uncorrelated to the dilepton direction. The softness of the missing transverse momentum distribution for $bbjj$ events, after the contour cuts of Eq. (9), is demonstrated in Fig. 2. The remaining $bbjj$ background can be eliminated by a cut

$$\not{p}_T > 20 \text{ GeV} \qquad \text{provided } p_{TH} < 50 \text{ GeV} . \tag{10}$$

Small $\not{p}_T$ and small $p_{TH}$ values are largely uncorrelated in the signal and the other backgrounds, resulting in a minimal effect of this cut (see the third column of Table I).

The background is dominated by $t\bar{t}j$ production, i.e. events where one of the two tagging jets is produced by a $b$-quark from top-decay. In many cases this jet will be observed in the central region of the detector, $|\eta_b| < 2.5$, where efficient $b$-tagging will be available. Since the tagging jets of the signal arise from light quarks, any events with $b$-tagged tagging jets should be eliminated. We assume a $b$-tagging efficiency of 60% for $b$-jets of $p_{Tb} > 20$ GeV in the central region ($|\eta_b| < 2.5$). This central $b$-veto reduces the $t\bar{t}j$ background by a factor 1.6 and is included in the $t\bar{t}$+jets cross sections of the tables and in the figures. The true $t\bar{t}j$,$t\bar{t}jj$ rejection rate will probably be larger, as $b$-quarks of $p_{Tb} < 20$ GeV can also be recognized via vertex information, although at reduced efficiency. Another net gain should arise from vetoing against leptons from semileptonic $b$ decays. Our estimates for the backgrounds involving $b$ quarks in the final state are conservative, since we do not include these additional rejection factors.

A further suppression of QCD backgrounds is achieved by a veto on any additional central jet activity, i.e. for any jets within the region defined by Eq. (4). In our previous analyses we have estimated an acceptance of 89% for the WBF signal, 75% for the EW backgrounds and 29% for the remaining $t\bar{t}$ and

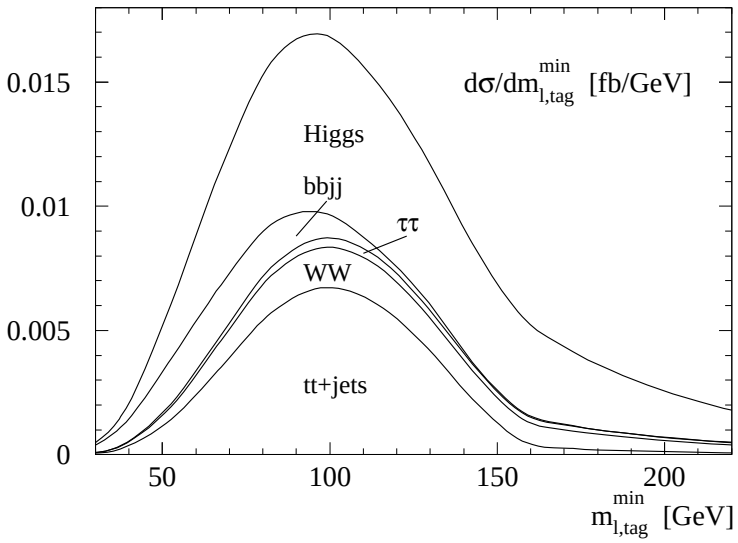


FIG. 3. Distribution of the smallest invariant mass of a tagging-jet and a charged-lepton, after the cuts of Eqs. (1–9). The areas between curves represent the contributions from the various background classes, as indicated, and the signal. QCD and EW backgrounds and the $t\bar{t}$ backgrounds have been combined for clarity.

other QCD backgrounds [4,5]. These suppression factors are included in the fourth column of Table I and in all figures.

In events where one of the tagging jets arises from $t \to bl\nu$ decay, the invariant mass of the charged lepton and the $b$-quark jet must be smaller than the top-quark mass, more precisely $m^2_{lb} < m^2_t - m^2_W$. Even though one will not know which pair of charged lepton plus tagging jet arises from decay of a top-quark, the smallest of the four possible combinations, $m^{\rm min}_{l,tag}$, has to be below this threshold. This effect is clearly visible for the $ttj$ background in Fig. 3 where we show $d\sigma/dm^{\rm min}_{l,tag}$ for various combinations of backgrounds and the sum of signal plus backgrounds. The region $m^{\rm min}_{l,tag} > 155$ GeV has a very small contribution from top-quark backgrounds and a much improved S/B ratio could be obtained by a cut. However, neither the significance of the signal nor the accuracy of a cross section determination would be improved by such a cut and therefore we do not consider it any further. The $m^{\rm min}_{l,tag}$ distribution contains valuable information for a neural net analysis, however, in particular for somewhat larger Higgs boson masses.

The cleanest evidence of the signal, and unambiguous information on the Higgs boson mass, will be visible in the $WW$ transverse mass distribution, which is shown in Fig. 4. The signal is observed as a clear Jacobian peak just below $M_T(WW) = m_H$. One should note that the $WW$ transverse mass and the dilepton mass are strongly correlated. From Eq. (7) one immediately finds $M_T(WW) > 2m_{ll}$. Thus, with $M_T(WW)$ cuts as indicated by the vertical lines in Fig. 4, the $m_{ll} < 60$ GeV requirement of Eq. (5) is almost automatically fulfilled. The $m_{ll}$ cut does have a strong effect on the high $M_T(WW)$ range in Fig. 4, however.

So far we have only considered the case of two different lepton flavors, i.e. $H \to WW \to e^\pm\mu^\mp \not{p}_T$. Our analysis can be carried over to $e^+e^-\not{p}_T$ and $\mu^+\mu^-\not{p}_T$ signatures with only minor modifications. Because of the dilepton invariant mass cut, $m_{ll} < 60$ GeV, leptonic $Z$-decays do not pose a large problem. However, low mass $l^+l^-$ pairs from $\gamma^* \to ll$ have a large cross section and we thus need to

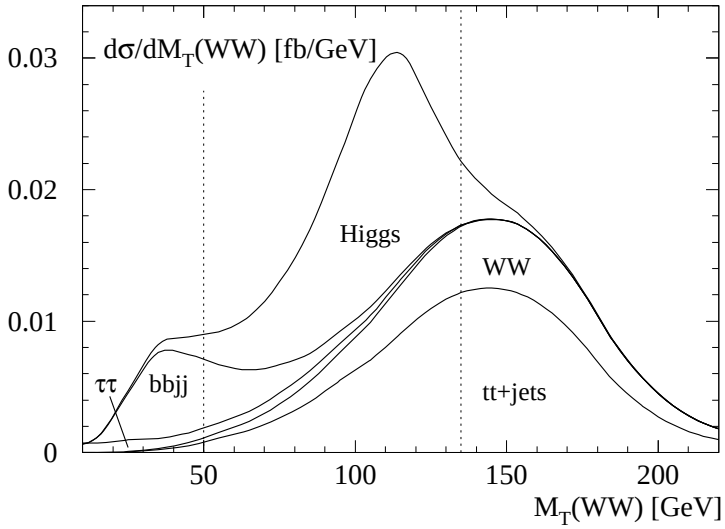


FIG. 4. $WW$ transverse mass distribution, $d\sigma/dM_T(WW)$, after the cuts of Eqs. (1–9) for $e\mu\not{p}_T$ events. The areas between curves represent the contributions from the various background classes and the signal, as indicated. The $bbjj$ background is effectively eliminated by the cut of Eq. (10) with minimal effect on the signal or the other backgrounds.

impose a minimum $m_{ll}$ cut, which we choose as 10 GeV. The dominant additional background then arises from $lljj$ events where missing transverse momentum is generated by detector effects. The contribution of this background to the $\not{p}_T$ distribution is shown as the dashed line in Fig. 2. It is tolerable above $\not{p}_T = 30$ GeV. For the same flavor case we, thus, impose the additional cuts

$$m_{ll} > 10 \text{ GeV} , \qquad \not{p}_T > 30 \text{ GeV} . \tag{11}$$

The resulting signal and background cross sections, including acceptance factors for the central jet veto, are listed in the last column of Table I.

The cross sections obtained in Table I can be translated into a "reach" of LHC experiments for measuring $H \to WW$ in WBF. Quantities of interest are the minimal luminosity required for a $5\sigma$ observation and the statistical accuracy with which the Higgs signal can be determined. For a realistic estimate we need to include additional detector effects. As in our previous analyses we assume lepton identification efficiencies of 0.95 for each central lepton and jet reconstruction efficiencies of 0.86 for each of the forward tagging jets, i.e. the cross sections in Table I need to be multiplied by an overall efficiency factor of 0.67. Note that geometric acceptance factors are already included in the parton level cross sections of Table I.

In Table II we separately show the Higgs signal and backgrounds for the $e\mu\not{p}_T$ and the same flavor samples, for Higgs boson masses between 110 and 140 GeV. The reach of the LHC is given in the last two columns and combines the information of the two samples. The $5\sigma$ discovery luminosity is determined using Poisson statistics for the small event numbers expected in the initial samples. The last column gives the statistical error, $\sqrt{S+B}/S$ which can be expected once both ATLAS and CMS have collected 100 fb$^{-1}$ each. The numbers assume a total data set of 200 fb$^{-1}$ and thus directly complement the numbers given in Table VI of Ref. [6] for the $H \to WW$ decay mode in WBF.

TABLE II. Expected cross sections times detection efficiencies (in fb) for a variety of Higgs boson masses. The first two columns represent the signal S and the sum of all backgrounds, B, as listed in the fourth column of Table I for the $e\mu\not{p}_T$ sample, i.e. the cuts of Eqs. (1–10) are included. Columns three and four list analogous results for the $l^+l^-\not{p}_T$ case, i.e. within the cuts of Eqs. (1–11). Column five lists the minimal integrated luminosity required for a $5\sigma$ signal and the last column gives the expected statistical error for the determination of $B\sigma(qq \to qqH,\ H \to WW)$ with 200 fb$^{-1}$ of data.

| | $H \to WW \to e^{\pm}\mu^{\mp}\not{p}_T$ | | $H \to WW \to e^+e^-,\ \mu^+\mu^- + \not{p}_T$ | | | |
|---|---|---|---|---|---|---|
| $m_H$[GeV] | $S$ | $B$ | $S$ | $B$ | $5\sigma\ \int \mathcal{L}$dt [fb$^{-1}$] | accuracy |
| 110 | 0.30 | 0.43 | 0.21 | 0.39 | 95 | 16.0% |
| 115 | 0.55 | 0.49 | 0.39 | 0.45 | 35 | 10.3% |
| 120 | 0.93 | 0.54 | 0.69 | 0.50 | 15 | 7.1% |
| 125 | 1.42 | 0.60 | 1.08 | 0.55 | 8 | 5.4% |
| 130 | 2.10 | 0.66 | 1.60 | 0.61 | 4 | 4.3% |
| 140 | 3.41 | 0.78 | 2.72 | 0.72 | 2 | 3.2% |

In conclusion, we find that even for a SM Higgs boson mass of 115 GeV, the WBF signal has characteristics which are sufficiently different from the backgrounds to allow extraction of a $H \to WW \to l^+l'^-\not{p}_T$ signal with $S/B \approx 1/1$ with a total signal acceptance of about 7%. This represents a substantial improvement over our earlier analysis [4] which arrived at a factor of 1.6 smaller signal rate for the $e\mu\not{p}_T$ final state, with $S/B \approx 0.6$. The main reasons for the improved results are i) optimization for lower Higgs boson masses, in particular the lowering of $m_{ll}$ and lepton $p_T$ cuts; ii) making use of correlations between lepton and missing $p_T$ directions; iii) inclusion of same flavor final states, i.e. $e^+e^-\not{p}_T$ and $\mu^+\mu^-\not{p}_T$ final states. In addition, the simulation of the dominant background, $t\bar{t}j$ production, has been improved by including all off-shell contributions, which raises this background by about 25%.

The final result is highly promising. 35 fb$^{-1}$ should be sufficient for a $5\sigma$ Higgs boson signal in the $qq \to qqH,\ H \to WW$ channel alone, for $m_H = 115$ GeV. This required integrated luminosity drops very quickly for somewhat higher mass values. At face value, this weak boson fusion mode performs better than the inclusive $H \to \gamma\gamma$ search, for which an integrated luminosity of 45 (70) fb$^{-1}$ will be required for a $5\sigma$ signal in CMS [7] (ATLAS [8]). Additional detector effects may lower these expectations somewhat. On the other hand, the weak boson fusion signal possesses a wealth of characteristics which can be exploited even better in a neural net analysis. $H \to WW$ in WBF now appears to be the most promising single channel for detection of a SM Higgs boson at the LHC.

## ACKNOWLEDGMENTS

This research was supported in part by the University of Wisconsin Research Committee with funds granted by the Wisconsin Alumni Research Foundation and in part by the U. S. Department of Energy under Contract No. DE-FG02-95ER40896. Fermilab is operated by URA under DOE contract No. DE-AC02-76CH03000.

# REFERENCES


[1] P. Igo-Kemenes, LEP seminar, CERN, Nov.3, 2000; R. Barate *et al.* [ALEPH Collaboration], hep-ex/0011045; M. Acciarri *et al.* [L3 Collaboration], hep-ex/0011043.

[2] H. E. Haber and R. Hempfling, Phys. Lett. **D48**, 4280 (1993); M. Carena, J.R. Espinosa, M. Quiros, and C.E.M. Wagner, Phys. Lett. **B355**, 209 (1995).

[3] S. Heinemeyer, W. Hollik and G. Weiglein, Phys. Rev. **D58**, 091701 (1998); R.-J. Zhang, Phys. Lett. **B447**, 89 (1999).

[4] D. Rainwater and D. Zeppenfeld, Phys. Rev. **D60**, 113004 (1999), Erratum-ibid. **D61**, 099901 (2000).

[5] D. Rainwater, PhD thesis, hep-ph/9908378.

[6] D. Zeppenfeld, R. Kinnunen, A. Nikitenko and E. Richter-Was, Phys. Rev. **D62**, 013009 (2000).

[7] G. L. Bayatian *et al.*, CMS Technical Proposal, report CERN/LHCC/94-38 (1994); R. Kinnunen and D. Denegri, CMS NOTE 1997/057; R. Kinnunen and A. Nikitenko, CMS TN/97-106; R.Kinnunen and D. Denegri, hep-ph/9907291.

[8] ATLAS Collaboration, ATLAS TDR, report CERN/LHCC/99-15 (1999).

[9] N. Kauer and D. Zeppenfeld, preprint MADPH-00-1205.

[10] T. Plehn, D. Rainwater and D. Zeppenfeld, Phys. Rev. **D61**, 093005 (2000).

[11] R. N. Cahn, S. D. Ellis, R. Kleiss and W. J. Stirling, Phys. Rev. **D35**, 1626 (1987); V. Barger, T. Han, and R. J. N. Phillips, Phys. Rev. **D37**, 2005 (1988); R. Kleiss and W. J. Stirling, Phys. Lett. **200B**, 193 (1988); D. Froideveaux, in *Proceedings of the ECFA Large Hadron Collider Workshop*, Aachen, Germany, 1990, edited by G. Jarlskog and D. Rein (CERN report 90-10, Geneva, Switzerland, 1990), Vol II, p. 444; M. H. Seymour, *ibid*, p. 557; U. Baur and E. W. N. Glover, Nucl. Phys. **B347**, 12 (1990); Phys. Lett. **B252**, 683 (1990).

[12] V. Barger, K. Cheung, T. Han, and R. J. N. Phillips, Phys. Rev. **D42**, 3052 (1990); V. Barger *et al.*, Phys. Rev. **D44**, 1426 (1991); V. Barger, K. Cheung, T. Han, and D. Zeppenfeld, Phys. Rev. **D44**, 2701 (1991); erratum Phys. Rev. **D48**, 5444 (1993); Phys. Rev. **D48**, 5433 (1993); V. Barger *et al.*, Phys. Rev. **D46**, 2028 (1992).

[13] D. Dicus, J. F. Gunion, and R. Vega, Phys. Lett. **B258**, 475 (1991); D. Dicus, J. F. Gunion, L. H. Orr, and R. Vega, Nucl. Phys. **B377**, 31 (1991).

[14] Y. L. Dokshitzer, V. A. Khoze, and S. Troian, in *Proceedings of the 6th International Conference on Physics in Collisions*, (1986) ed. M. Derrick (World Scientific, 1987) p.365; J. D. Bjorken, Int. J. Mod. Phys. **A7**, 4189 (1992); Phys. Rev. **D47**, 101 (1993); V. Barger, R. J. N. Phillips, and D. Zeppenfeld, Phys. Lett. **B346**, 106 (1995).

[15] D. Rainwater, R. Szalapski, and D. Zeppenfeld, Phys. Rev. **D54**, 6680 (1996).

[16] M. Dittmar and H. Dreiner, Phys. Rev. **D55**, 167 (1997); and [hep-ph/9703401].

[17] R. K. Ellis, I. Hinchliffe, M. Soldate and J. J. van der Bij, Nucl. Phys. **B297**, 221 (1988).